Experimental investigation of starting-up, energy-saving, and emission-reducing performances of hybrid supercapacitor energy storage systems for automobiles

Qinchao Zhang [a], Liangde Liu [a,*], Jiangyun Zhang [a,**], Guoqing Zhang [a], Youpeng Chen [b], Sizhi Liu [c], Hongwei Wu [d], Hongni Huang [a]

a School of Materials and Energy, Guangdong University of Technology, Guangzhou, Guangdong, 510006, China

b School of Intelligent Engineering, Guangzhou Nanyang Polytechnic Vocational College, Guangzhou, Guangdong, 510900, China

c Dongguan Gonghe Electronics Co., Ltd, Dongguan, Guangdong, 523808, China

d School of Physics, Engineering and Computer Science, University of Hertfordshire, Hatfield, AL10 9AB, United Kingdom

ABSTRACT

Improvements in engine starting-up performance, such as reducing fuel consumption and exhaust emission pollution during the startup process, are very vital to achieve the national development goal of carbon peaking and carbon neutrality. Hybrid supercapacitor (HSC) energy storage systems containing batteries and supercapacitors (SCs) are considered promising energy storage strategies to compensate for the disadvantages of a single energy storage technology. In this paper, two kinds of novel 12 V/50 Ah and 12 V/70 Ah module-level energy storage systems were first composed of cell-level 3.6 V/2200 F HSCs were designed. Analysis on their fundamental electrochemical properties under room temperature conditions was also performed. Four different types of energy storage systems composed of 12 V/70

---

*Corresponding author

**Corresponding author.

E-mail addresses: Liangdeliugdut@163.com (L. Liu), roseyyun@163.com (J. Zhang)

Ah lithium iron phosphate (LFP) batteries, 12 V/70 Ah valve-regulated lead-acid (VRLA) batteries, and the aforementioned HSCs were then employed to compare their starting energy, energy-saving, and emission-reduction characteristics. Additionally, the 12 V/70 Ah HSC module saved 7.82%, 3.18%, and 1.65% of fuel as compared to the 12 V/70 Ah VRLA, 12 V/70 Ah LFP, and 12 V/50 Ah HSC modules, respectively, demonstrating its superior fuel economy property. Simultaneously, the volume concentration of HC and CO emission in the startup process are 12.7% and 13.2% lower than that average of the other three modules, respectively, which shows a good exhaust emission reduction effect. The proposed energy storage system will provide systematic experimental data support and valuable theoretical guidance for the industrialization and application of HSCs.

***Keywords*:**

Hybrid supercapacitors, energy storage systems, starting-up, energy saving, and emission reduction

1. Introduction

In 2020, China had a transportation carbon emission of 930 million tons. Road transport accounted for 90% of total carbon emissions in the entire transportation sector, which road passenger transport accounted for 42% of; furthermore, 90% of that came from passenger cars alone [1-3]. This also causes a large amount of fuel consumption, among which, insufficient fuel combustion leads to a series of exhaust emission pollution [4]. Hence, it is particularly important to improve the performance of energy-saving and emission reduction of fuel trucks during ignition. In general, frequent start-up processes generate severe fuel consumption and exhaust emission problems [5,6]. Additionally, traditional automotive energy storage systems, such as valve-regulated lead-acid (VRLA) batteries, exhibit excessive voltage drops during the starting process, short service life, and poor, low-temperature starting performance [7,8]. Moreover, lithium iron phosphate (LFP) batteries exhibit safety risks and other shortcomings during high-temperature startups [9,10]. The hybrid supercapacitor (HSC) is a novel, environmentally friendly energy storage system composed of a high-rate, double-layer capacitive positive electrode and large-capacity battery-type negative electrode [11-13]. It has become a research hotspot due to its high power supercapacitor (SC) density and high battery energy density [14-17]. HSCs integrate the energy storage mechanism of double-layer capacitors and the energy storage mechanism of batteries. One pole adopts a battery-type electrode to store energy through the embedding and removal of metal ions in the electrode material lattice, while the other pole adopts a double-layer capacitor electrode to store energy through the absorption and desorption of ions on the electrode material surface [18-21]. Furthermore, current self-charging SCs [22], multi-responsive healable SCs [23] and foldable quasi-solid-state SCs are also widely used in flexible wearable energy storage devices [24]. These emerging SCs have high potential in the next generation of portable electronic devices.

Since HSCs have a higher working potential and larger capacitance to meet the starting power, they can also undergo long-term starting without charging, have fast charge-discharge ability, a long cycle life, and can withstand extreme low- and high-temperature environmental conditions [25,26] while maintaining their small internal resistance, low self-discharge, short circuit without explosions, safety, and environmental protection [27-29]. Consequently, HSCs are more advantageous than using batteries or SCs alone as a vehicle energy storage system [30,31]. As compared to the composite power supply, it is unnecessary to use an SC in series or parallel with a VRLA or LFP battery, thus saving space, simplifying the design, and lowering the long-term cost [32-35].

HSC energy storage systems have been increasingly researched in recent years. For example, Sun et al. [36-38] comprehensively reviewed the preparation method and electrochemical performance of $CuCo_2O_4$-based HSC materials, which provided valuable theoretical guidance for the engineering applications of HSCs. Shao et al.

[39-43] studied graphene as the anode material of lithium-ion HSCs and verified its high energy and excellent high-power properties. Chen et al. [44-46] prepared nickel foam-supported $MnCo_2O_{4.5}$ porous nanowires with high-performance HSCs electrodes, showed an impressive cyclic stability, and reviewed the progress of the application research of $MgCo_2O_4$-based composites in SCs. Yin et al. [47] fabricated $(Ni,Co)Se_2$ nanoparticles on vertical graphene nanosheets@carbon microtubes membrane electrode for HSCs exhibits excellent electrochemical performance in terms of high specific capacitance (1740 F g^{-1} at 1 A g^{-1}), good rate capability (71.8% capacitance retention at 20 A g^{-1}), and superior cycling stability (89.6% capacitance retention after 10,000 cycles). Liu et al. [48,49] explored the engine starting performance of composite energy storage systems based on SCs. Their results exhibited shorted engine starting times and improved engine starting performance. Guo et al. [50,51] designed a 48 V LI ion capacitor start-stop power system, the results of which indicated that the vehicle had very good fuel economy during startup. Yu et al. [52-55] proposed a composite power supply combining battery and SC. The bench test showed that the composite energy storage system provided a greater starting current and improved starting power compared with lead-acid batteries. Zhang et al. [56-59] studied the composite energy storage system composed of lead-acid battery and lithium titanate battery in parallel, the results of which showed that the composite energy storage system was conducive to improving the cycle life of lead-acid battery and optimizing energy-saving effects and emission reduction. Liu et al. [60-62] examined a new hybrid power system of 42 V vehicle batteries and SCs and verified the effectiveness and reliability of hybrid power through Matlab/Simulink simulations and experiments. Gong et al. [63-66] established a composite energy storage system composed of HSCs and batteries for simulation and experimental research, which improved the voltage drop of battery and greatly improved the starting performance.

Having said all of the above, the existing hybrid energy storage system for vehicle startup is mainly composed of SCs combined with VRLA batteries as well as lithium batteries in series and parallel mode. As a result, these give full play to the high-power rate of SCs and high energy of batteries, which is faster and more fuel-efficient than a single energy storage system [67,68]. However, few scholars have conducted comparative and experimental studies on the starting performance of HSCs and batteries, especially the comparative analysis of starting fuel consumption and starting exhaust gas [69,70]. Hence, the design of an energy storage system with battery and SC performance by HSC is of urgent need.

Based on the combination of supercapacitor and battery energy storage system, this paper proposed an energy storage system module built at the cell level of HSCs, of which the starting performance, fuel consumption, and exhaust emission effects of the vehicle were examined. First, two HSC energy storage systems were designed; their electrochemical properties were tested. Second, the HSCs based on engine test benches were compared with the start of the battery test. Third, the start fuel consumption and exhaust gas of HSCs and batteries were compared. The experimental results showed that the HSC energy storage system had a significantly shorter startup time and resulted in less frustration than other types of battery modules. Additionally, the performance in terms of fuel saving and emission reduction was remarkable, and the fuel economy was improved. In the future, with the rapid development of automobile industry and transportation industry, people have put forward higher requirements for automobile energy conservation, emission reduction and safety performance. The development of an HSC energy storage system with high efficiency that saves energy and is environmentally friendly is expected to replace the traditional VRLA and LFP battery energy storage systems; this will be conducive to improving the quality of vehicle starting performance. Moreover, the low long-term cost of the HSC energy storage system has played an important role in accelerating its promotion and application and advancing its industrial development. As such, the promotion of its industrial development has important significance and application value.

2. Experimental design

2.1. Selection of HSC monomers

Before the design of the energy storage system, the 18650 type 3.6 V/2200 F HSCs from Dongguan Gonghe Electronics Co., Ltd. was selected based on the voltage, capacity, safety, and cost of the starting power supply. Its internal structure included an electrode sheet, isolation film, pole, and shell. In addition, the coating on the electrode sheet included an active material, conductive agent, and adhesive [71-74]. The active material was a mixture of various materials, including carbon material, conductive polymer, and graphite-type carbon nitride. The carbon material had a core-shell structure [75,76], and its nuclear layer included graphene fiber and carbon nanotubes. Its shell was composed of a functional layer of manganese dioxide [77-79]. The conducting polymer was a mixture of polyaniline, polythiophene, and polypyrrole [80-84]. Composites of carbon materials and conductive polymers combine the best of both types of materials and exhibit synergistic effects. The conductive polymer provides the HSC, and the carbon material acts as the skeleton in the complex, supporting the conductive polymer to maintain its stability during the charging and discharging cycle. [85-89]. The technical parameters (e.g., monomer) are presented in Table 1. The Service life test data in the table were conducted by China CEPREI Laboratory under the following experimental conditions (ambient temperature: 20°C±5°C, relative humidity: 25%–85%, ambient pressure: 86–106 kPa). The corresponding test steps are as follows:

Step 1: Choosing 3 samples, using a constant voltage charging method, charge with 0.5 A constant current to the rated voltage 3.6 V, until the current drops to 50 mA.

Step 2: The charged samples stored in an ambient for 5 minutes.

Step 3: Discharge at 0.5 A current to 2 V cut-off voltage.

Step 4: The discharged samples stored in an ambient for 5 minutes.

Step 5: Charge with 0.5 A constant current to the rated voltage 3.6V, until the current drops to 50 mA.

Step 6: Step 2 to 5 repeated at least 300 times (one time defined as one cycle).

After testing according to the above steps, the total cycle number, N, is calculated using the following (1):

$$N = \frac{C_0}{C_0 - C_n} \times n \times \left(\frac{I}{10}\right)^2 \times 80\% \qquad (1)$$

Where, C_0 is the initial discharge capacity, Ah; C_n is the remaining discharge capacity after cycle test, Ah; n is the completed cycle number, times; I is the constant discharge current in the cycle test, I = 0.5 A.

The calculation results show that the 3.6 V/2200 F HSC cells have no less than 80% capacity after more than 20000 cycles.

Table 1 Technical specifications parameters of the HSC monomer.

Descriptions	Specification	Conditions
Nominal voltage (V)	3.6	
Nominal capacity (F)	2200	Standard discharge current
Capacity tolerance	±20%	Standard discharge current
Maximal recharging voltage (V)	3.65	
Maximal charging current (mA)	2000	
Discharge cut-off voltage (V)	2	
Maximal discharging current (mA)	6000	Pulse current discharge 30 A
Using temperature scope (°C)	−30–70	
Storage environment temperature (°C)	−20–65	
Storage environment humidity	≤ 85%	
Weight (g)	40	
Internal impedance (mΩ)	≤ 28	Upon fully charge (1 kHz)
Service life (times)	≥ 20000	Not less than 80% capacity
Size (mm)	65×Φ18	
Protection class	IP 30	

2.2. Assembly of HSC energy storage system

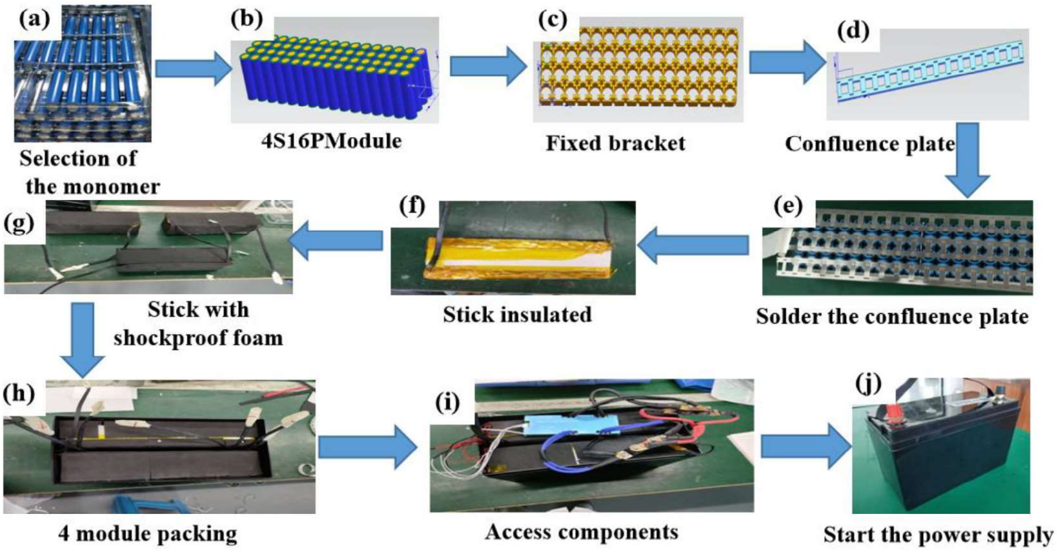

Fig. 1. Design flow chart of energy storage system of HSCs: (a) selection of the monomer; (b) 4S 16PModule; (c) fixed bracket; (d) confluence plat; (e) solder the confluence plate; (f) stick insulated; (g) stick with shockproof foam; (h) 4 module packing; (i) access components and (j) energy storage system.

The independent design hybrid super capacitor starting power assembly process is shown in Fig. 1. First, the selection of voltage difference value was less than 30 mV, such that poor internal resistance value was less than 0.1 mΩ in the monomer. In addition, the 4S 16P monomer had a fixed bracket, spot welder welding junction formation module, an insulated module, and a welding wire. Second, stick was composed of shockproof foam. Finally, the four modules were packed and connected to the BMS, diodes, weak current switches, and other accessories, thereby generating the HSC module energy storage system. The system was designed with a rated voltage of 12 V and a rated capacity of 70 Ah. Furthermore, a 12 V/50 Ah HSC module was composed of four 4S 12P modules and was designed in the same way. Its technical specifications are shown in Table 2. The technical parameters of the purchased LFP battery and Camel VRLA battery from Guangzhou Geyu Electronics Co., Ltd. are shown in Table 3.

Table 2 Technical specifications parameters of the energy storage system independent designs.

Specifications	12 V/50 Ah HSCs	12 V/70 Ah HSCs
Serial mode	4S 48P	4S 64P
Storage capacity (Ah)	50	70
Rated voltage (V)	12	12
Maximum charging voltage (V)	14.4	14.4
Internal resistance (mΩ)	22.31	20.12
Product weight (kg)	11.24	13.8
Operating temperature (°C)	−30–70	−30–70
Service life (times)	≥ 20000 (Not less than 80% capacity)	≥ 20000 (Not less than 80% capacity)
Product size (mm)	255×165×215	325×165×215
Protection class	IP 30	IP 30

Table 3 Technical specification parameters of the purchasing energy storage systems.

Specifications	12 V/70 Ah LFP batteries	12 V/70 Ah VRLA batteries
Serial mode	4S 3P	6S 1P
Storage capacity (Ah)	70	70
Nominal voltage (V)	12	12
Maximum charging voltage (V)	14.6	16
Self-discharge	5%	10%
Product weight (kg)	8	14.78
Operating temperature (°C)	−20–55	−10–60
Product size (mm)	278×175×190	250×160×200
Protection class	IP 30	IP 30

2.3. Constructing experimental test platform

2.3.1. Fundamental electrochemical performance test platform

Fig. 2. Test platform for the electrochemical performance of HSC energy storage systems.

The electrochemical performance test platform of the energy storage systems of HSCs are presented in Fig. 2. This platform was mainly composed of a special battery charge/discharge aging machine and a data analysis system. Its technical parameters are shown in Table 4. It was used to test the charge/discharge voltage and capacity variation characteristics of the energy storage systems of HSCs. The crocodile clip of the test line of the battery charging/discharging aging special machine was connected to the positive and negative poles of the starting power of the HSCs to conduct the charging/discharging test of the starting power of the HSCs. In addition, the data analysis system was connected to the battery charge/discharge aging special machine for experimental data transmission, storage, and analysis.

Table 4 Technical specifications parameters of electrochemical test platform.

Laboratory equipment	specification
Battery charging/discharging special aging machine	Voltage range: 0–100 V Charging current: 0–10 A Discharge current: 0–20 A Charge constant voltage cut-off current: < 10 mA Charging mode: Constant current and constant voltage charging Discharge patterns: Constant exile electric Charging cut-off condition: Voltage, current, relative time, overcharge protection Discharge cut-off conditions: voltage, relative time, over-discharge protection

	Cycle range: 1–999 times
	Precision: ± 1 ‰

2.3.2. Startup performance test platform

Fig. 3 presents the experimental platform for testing the startup performance of HSCs and batteries. The experimental platform included: the technical parameters of the engine test bench, 12 V/50 Ah HSCs module, 12 V/70 Ah HSCs module, 12 V/70 Ah LFP batteries module, 12 V/70 Ah VRLA batteries module, BMS, communication box, PC host computer, and noise tester (Table 5). Among them, the 2017 Magiten B8 engine test bench (Guangzhou Wangzhong Education and Technology Co., Ltd.) was included. The 12 V/70 Ah HSCs module was installed on the test bench, and BMS was connected to collect the voltage, current, temperature, and SOC estimation. The data was transmitted to the PC upper computer by connecting the UART communication box, and the PC upper computer received the data and stored it. Additionally, the noise was tested by the noise tester. The same scheme was used to replace the 12 V/70 Ah HSC module with the 12 V/50 Ah HSC module, the 12 V/70 Ah LFP battery module, and the 12 V/70 Ah VRLA battery module for experiments. All experiments were carried out on the same experimental bench. Finally, the data of the test platform in this experiment was compared, from which the peak starting current, voltage drop, and instantaneous power change of the four energy storage systems were analyzed. The starting effect was then studied, and the startup capability was analyzed by a comparison with the startup noise.

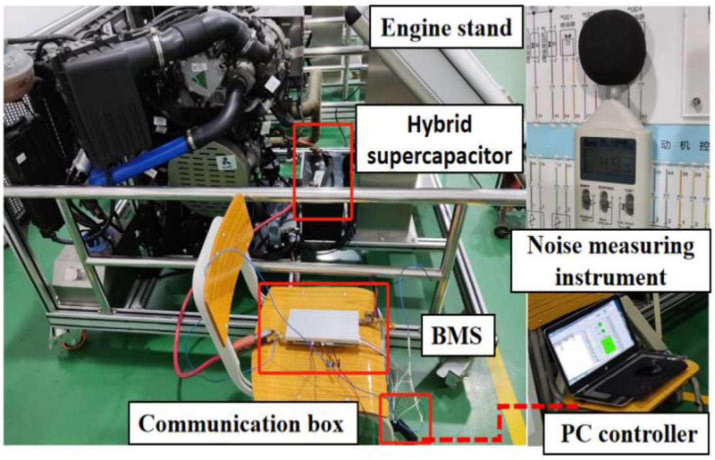

Fig. 3. HSCs and batteries startup performance test platform.

Table 5 Technical specifications parameters of startup performance experimental equipment.

Laboratory equipment	Specification
Engine test bench	Specifications and models: 2017 B8 Volkswagen Magotan 2.0T-EA888
	Maximum horsepower: 220 Ps
	Maximum torque: 350 Nm
	Transmission: 7-speed wet dual clutch
BMS	Model and specification: JBD-SP04S034
	Cell specification: 3–4 string
	Port type: Charge and discharge with the same port
	Single voltage: 2.2–3.75 V
	Continuous discharge current: ≤ 250 A
	Power consumption: ≤ 25 mA
	Internal resistance of the protection plate: ≤10 mΩ
	Operating temperature: −30°C–70°C
Communication box	UART communication
Noise measuring instrument	Model and specification: SL-1350 B
	Measurement range: Lo=35–100 dB/ Hi = 65–130 dB

2.3.3. Fuel consumption test platform

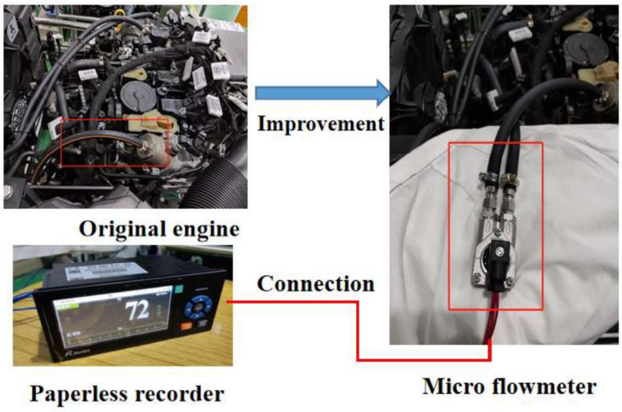

Fig. 4. HSCs and batteries startup fuel consumption test platform.

Fig. 4 presents the experimental test platform for starting fuel consumption. The test instruments and equipment of this experimental test platform included: 2017 Magiten B8 engine test bench, 12 V/50 Ah HSCs module, 12 V / 70 Ah HSCs module, 12 V/70 Ah LFP batteries module, 12 V/70 Ah VRLA batteries module, small oil consumption flowmeter, and paperless recorder developed by Axia Instrument Firm. This was placed in high-tech development zone. The device specifications are summarized in Table 6. The original engine was improved, and a small fuel consumption flowmeter was connected to the oil inlet pipe to collect the starting fuel consumption flow rate and cumulative fuel consumption. The collected data were output through a paperless recorder. This experimental test platform was used to study the starting time, fuel consumption flow rate, and cumulative fuel consumption of four different energy storage systems each time. Further analysis on the fuel consumption of the energy storage systems of the HSCs was performed every time.

Table 6 Technical specifications parameters of fuel consumption test equipment.

Laboratory equipment	specification
Micro-meter for fuel consumption	Type: GICAR
	Specification: 0.7 mm, 1.5–42 (L/h)
	Instrument coefficient: 0.3 (cm^3/imp), 3333 (I/L)
	Temperature range: −10–100°C
	Level of accuracy: ± 2%
	Accuracy of repetition: ± 0.2%

	Overall size: 40×55×40 mm
	Power supply: 4.5–24 VDC
	Output: Open collector circuit
Paperless recorder	Specifications and models: R6200-A06-R02-PA1-SU-MD-VAC
	Input: 220 VAC/50 Hz
	interface: USB1.1/2.0 U disk
	Precision grade: 0.5%
	Output signal: Pulse output, 4–20 mA output, RS485 output
	Medium temperature: −20–100°C
	Protection grade: IP 65 (Waterproof level)

2.3.4. Exhaust test platform

The exhaust gas experimental test platform was built according to the connection mode in Fig. 5. The test instruments and equipment of the platform included: technical specifications of 2017 Magton B8 engine test bench, 12 V/50 Ah HSCs module, 12 V/70 Ah HSCs module, 12 V/70 Ah LFP batteries module, 12 V/70 Ah VRLA batteries module, NHA-506 tail gas analyzer, and standard tail gas (Table 7). Among them, the tail gas analyzer was used to analyze the volume concentrations of HC, CO, and CO_2 in the starting process of four different energy storage systems, and the standard tail gas was used to calibrate the tail gas analyzer before starting. Through the experimental platform, the volume concentrations of HC, CO, and CO_2 in the startup exhaust gas of each energy storage systems were compared and studied. The exhaust emission performance of the energy storage systems of the HSCs was analyzed.

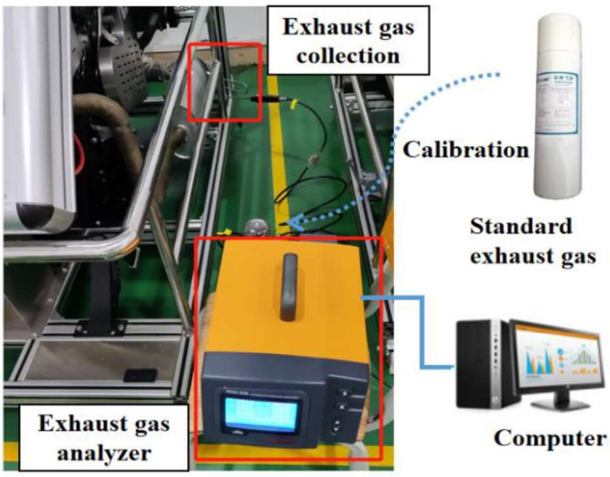

Fig. 5. HSCs and batteries startup exhaust test platform.

Table 7 Technical specifications parameters of exhaust test equipment.

Laboratory equipment	Specifications
Exhaust gas analyzer	Specification: NHA-506 Including instrument host, short catheter, prefilter, sampling tube, sampling probe, and embedded micro printer Implementation standard: "Q/NH4 Vehicle Emission Gas tester" Key components: Nitrogen and oxygen sensor, oxygen sensor, main control board, and optical platform Test principle: The principle of infrared absorption method The environment temperature: + 5°C–+ 40°C Relative humidity: 5%–95% (The condensation) Atmospheric pressure: 70 kPa–106 kPa HC (hexane equivalent) measurement range: (0–10000) x 10^{-6} vol CO measurement range: (0–10) x10^{-2} vol CO_2 measurement range: (0–18) x10^{-2} vol The relative error: ± 5% Warm up time: 10 minutes Output interface: RS-232C Overall dimensions (length × width × height): 450×260×180 mm Weight: 7 kg
Standard for exhaust gas	Gas standard number: GBW (E) 080449 C_3H_8 Component concentration: 0.314×10^{-2} CO Component concentration: 3.55×10^{-2} CO_2 Component concentration: 7.9×10^{-2}

2.4. Experimental test

2.4.1. Electrochemical performance testing

The electrochemical performance test experiment of the self-designed HSC energy storage systems was carried out at room temperature (25.6°C). First, the 12 V/50 Ah and 12 V/70 Ah HSC energy storage systems were divided into two groups. Second, the charging test of the energy storage system was performed. Before the test, the HSCs were discharged with a current of 20 A to a cut-off voltage of 9 V, and let stand for 30 min. They were then charged to 14.4 V with a current of 10 A. Finally, the discharge test of energy storage system was carried out. Before the test, the HSCs were charged with a current of 10 A to a rated voltage of 14.4 V, let stand for 30 min, and then discharged with a current of 20 A to a cut-off voltage of 9 V. Each group was tested 6 times, and the average value of the data was analyzed to draw the curve of voltage, capacity, and time. Moreover, the 12 V/70 Ah hybrid supercapacitor energy storage system module has been completed two charge-discharge cycle tests with 10A current. And Coulombic efficiency (η) of HSCs are calculated through the following Eq. (2) [90,91]:

$$\eta = \frac{C_d}{C_c} \times 100\% \qquad (2)$$

Where, C_d is the discharge capacity and C_c is the charging capacity.

2.4.2. Startup performance testing

The startup performance test was carried out at room temperature (26.2°C). The experimental object was 2017 Magotan B8 test bench, and the experiment was carried out according to the National Standard GB/T 18297-2001 "Automobile Engine Performance Test Method". First, the HSC module of 12 V/50 Ah and 12 V/70 Ah, the VRLA battery module of 12 V/70 Ah, and LFP battery module of 12 V/70 Ah were fully charged and allowed to stand for 30 min. During this period, the engine with the backup power supply was started and run at idle speed for a period of time to increase the temperature to normal working state. The engine was then shut down. The full of the start of the electric power were then conducted on the engine test bench to start the experiment. Four kinds of energy storage systems were divided into four groups for the experiment. Each group carried out 12 experiments, each including idle time launched for a total of 1 min. Before each start experiment, the energy storage system was fully charged to the rated voltage and let stand for 30 min. The average value was taken to draw the voltage and current curves. Furthermore, a noise tester was used to test the startup noise during the starting process. The ambient noise was 50.28 dB. The noise tester for each test was placed in the same position, and the data was recorded to draw a startup noise curve.

2.4.3. Startup fuel consumption testing

Startup fuel consumption experiment was conducted at room temperature (26.3°C) and followed the unified detection standard GB/T19233-2008 "Light Vehicle Fuel Consumption Test Method". The volume method was used to measure fuel consumption. As compared to the mass method, the operation of weighing fuel consumption was simpler, and the result was more accurate. According to the above starting performance test, the engine was preheated and the starting power was fully charged and let stand for 30 min. The four energy storage systems were divided into four groups for the experiment, wherein each group was started 25 times. Before each startup, the energy storage system was fully charged to the rated voltage and let stand for 30 min. The data were exported through the paperless recorder to analyze the fuel consumption flow rate and cumulative fuel consumption at each startup.

2.4.4. Startup exhaust testing

The startup exhaust test will be carried out at room temperature (26.2°C). The test was carried out according to the working principle and installation requirements of NHA-506 exhaust analyzer, and according to the national "Emission Limits and Measurement Methods of Exhaust Pollutants for Ignition Engine Vehicles with Double Idle Speed Method and Simple Working Condition Method". Before the test, the engine was allowed to heat. During the test, the tail gas analyzer was first preheated for 500 s. The air tightness and sensor aging were then checked, after which the standard gas calibration and zero calibration were performed. Finally, the sampling probe was inserted into the exhaust pipe and fixed. The four energy storage systems were divided into four groups for the experiment. Each group was started 12 times, and the engine was started and stopped at idle speed for 1 min each time. The data of the starting process was recorded and the volume concentration changes of HC, CO, and CO_2 were analyzed when starting from different energy storage systems.

3. Results and discussion

3.1. Electrochemical performance analysis

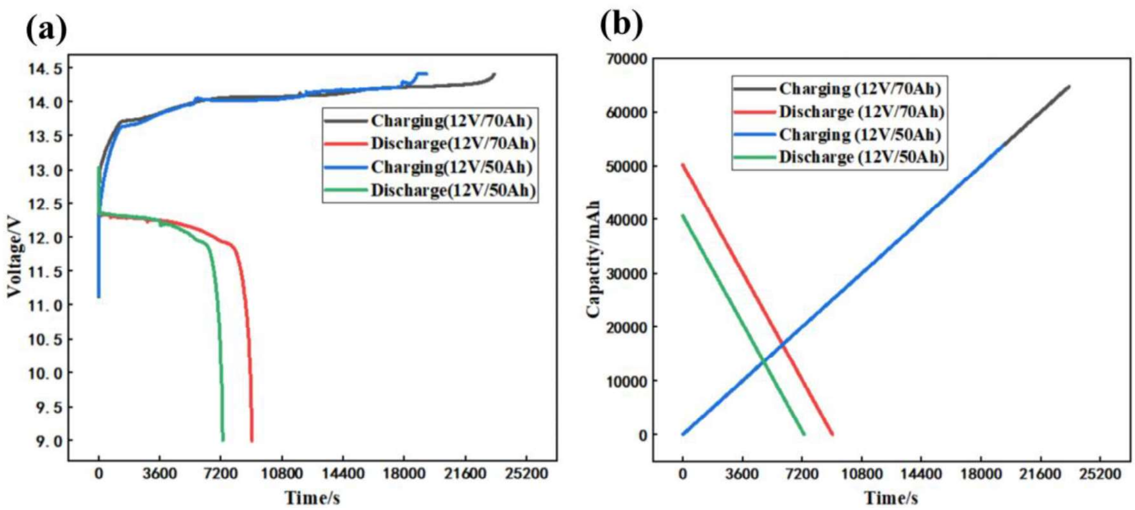

Fig. 6. Charge/discharge curves of HSCs: (a) voltage, and (b) capacity.

According to the above design requirements, one set of 12 V/70 Ah and one set of 12 V/50 Ah HSCs were assembled. In addition, the charge/discharge tests were completed. According to Fig. 6a, the voltage trends of charge/discharge of the two HSCs were consistent. In the charging stage, 10 A constant-current charging was adopted, and the voltage first jumped from 11.18 V to 12.48 V and then slowly increased to 14.4 V. This was due to the rapid charging characteristics of the HSC, which had a voltage jump change. In the discharge stage, 20 A constant current was used, and the voltage rapidly dropped from 13.10 V to 12.35 V, then slowly dropped, and finally exhibited a sharp drop to 9 V. These observations were due to the rapid voltage drop at the beginning of discharge, which is characteristic of HSCs. With the delay of the discharge time, the capacity decreased, thereby resulting in a sharp voltage drop. The analysis of the results in Fig. 6b show that the charging capacity of the 12 V/50 Ah HSCs was 53 Ah and the discharge capacity was 40 Ah. The charging capacity of the 12 V/70 Ah HSCs was 68 Ah, and the discharging capacity was 50 Ah. The discharging capacity was affected by the cut-off voltage of 9 V. Hence, the discharging capacity was smaller than the charging capacity. The actual capacity of the energy storage systems met the design requirements. Moreover, the 12 V/70 Ah HSCs energy storage system designed by us carried out two charge-discharge cycles at a current of 10 A, with each cycle of about 15 h. The average charged capacity is 68.625 Ah, the average discharged capacity is 68.108 Ah, and the Coulomb efficiency is 99.25%. It shows that charge storage rather than parasitic reaction is dominant.

3.2. Startup performance Analysis

To illustrate the startup advantages of the HSC energy storage systems, the energy storage systems of LFP batteries module and LFP batteries module were compared. In addition, changes in the starting voltage, current, instantaneous power, and startup noise were analyzed.

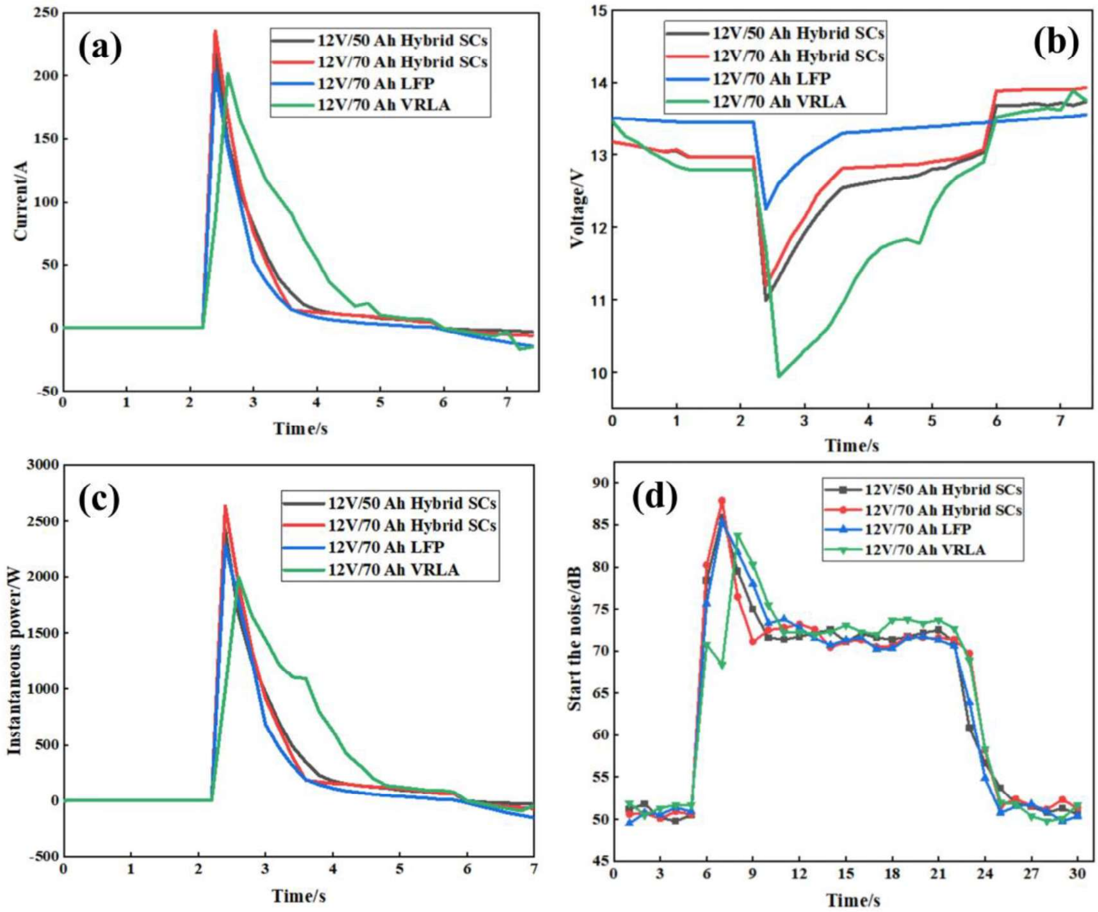

Fig. 7. Multiple starts curves of four energy storage systems: (a) average current; (b) average voltage; (c) average instantaneous power and (d) average noise.

The average current curves of the four power supplies during multiple starts are shown in Fig. 7a. The peak value appeared during the starting process. At this time, the engine starting motor drove the crankshaft to rotate. A large resistance moment and a low starting motor speed were observed, resulting in high current. The current on the right side of the peak current dropped slowly, indicating that the speed of the starting motor rose and the resistance decreased. The average current released by 12 V/70 Ah HSCs reached 240 A, which was larger than the average current released by 12 V/70 Ah LFP batteries module and VRLA batteries module of 200 A. The average release current of 12 V/50 Ah HSC was smaller than that of 12 V/70 Ah HSC. When the energy storage systems was finished, the generator charged the energy storage systems, thereby generating a negative current and producing slow and stable changes in the charging current of the HSC.

The average voltage curves of the four energy storage systems during multiple startups are elaborated in Fig. 7b. The voltage dropped rapidly during startup. The starting voltage of 12 V/70 Ah LFP batteries module dropped from 13.5 V to 12.3 V, and the average voltage declined to 1.2 V. The starting voltage of 12 V/70 Ah HSCs decreased from 13.2 V to 11.2 V, with an average voltage drop of 2 V, followed by 12 V/50 Ah HSCs. The VRLA batteries module startup voltage dropped from 13.4 V to 9.9 V, with an average voltage drop of 3.5 V reaching the maximum. In the charging stage, the voltage of 12 V/50 Ah and 12 V/70 Ah HSCs quickly rose and appeared higher than the initial voltage. In comparison, the voltage of 12 V/70 Ah LFP batteries module rose slowly, and the voltage of VRLA batteries module showed obvious fluctuations.

According to the analysis of the average instantaneous power of the four energy storage systems during multiple starting (Fig. 7c), the instantaneous power rose sharply at the beginning of startup. The 12 V/70 Ah HSC had a maximum average instantaneous power of 2700 W. In comparison, the average instantaneous power of 50 Ah HSC was small. However, it was relatively close to the average instantaneous power of 12 V/70 Ah LFP battery. The 12 V/70 Ah VRLA battery had a minimum average instantaneous power of 2000 W, and the average instantaneous power of the four energy storage systems gradually decreased. In addition, negative power was observed after startup indicating the start of charging.

According to the noise test of four energy storage systems in multiple starts (Fig. 7d), the maximum noise in the starting process of 12 V/70 Ah HSC was about 5 dB higher than that of 12 V/70 Ah VRLA battery module. In comparison, the average noise of the 12 V/70 Ah LFP battery module was close to that of the 12 V/50 Ah HSC. In addition, the average starting noise was less than that of the 12 V/70 Ah HSC. Under the condition that the rated torque was not exceeded, the 12 V/70 Ah HSC released a large current and showed a small voltage drop after starting, which then increased the instantaneous startup power and started engine torque augmentation. As such, the speed quickened, resulting in greater noise.

3.3. Startup fuel consumption analysis

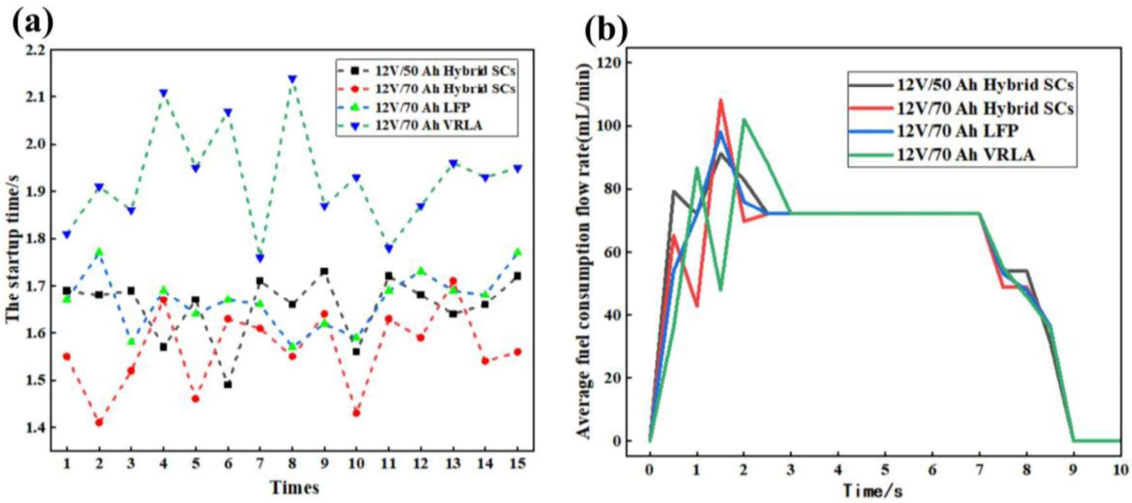

Fig. 8. Multiple starts curves of four energy storage systems: (a) startup time;, and (b) average fuel consumption flow rate.

Fig. 8a presents the time curves of the four energy storage systems during several startups. The starting time of the 12 V/70 Ah HSC was significantly shorter than that of the 12 V/70 Ah VRLA battery module. In addition, the starting time of the 12 V/50 Ah HSC and 12 V/70 Ah LFP battery module were slightly shorter than that of the 12 V/70 Ah VRLA battery module.

Fig. 8b shows the average fuel consumption flow rate curves of the four energy storage systems following several startups. The engine had an average fuel consumption flow rate of 72 mL/min in idle state and showed stable operation. In addition, the HSC exhibited a shorter average fuel consumption velocity fluctuation time.

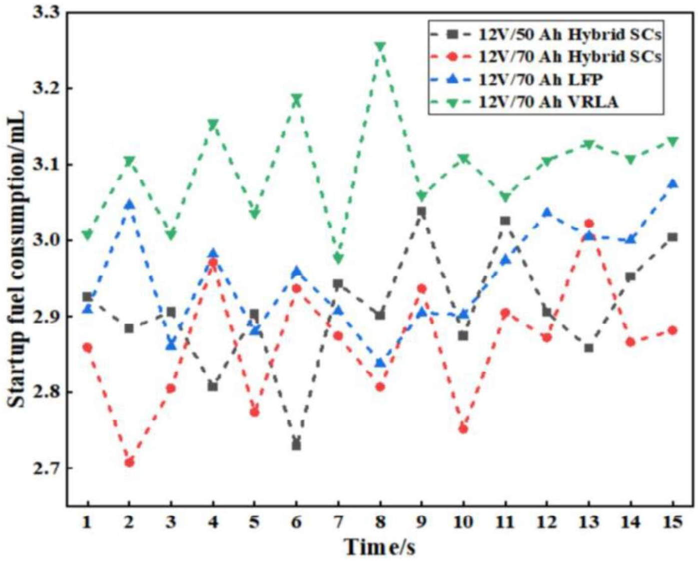

Fig. 9. Fuel consumption curves for multiple starts of four energy storage systems.

The starting fuel consumption curves of the four energy storage systems after several startups (Fig. 9) showed an average starting fuel consumption distribution for 12 V/70 Ah HSC of <2.9 mL. In comparison, the average starting fuel consumption distribution of the 12 V/70 Ah VRLA battery module was above 3.1 mL, indicating a change in the fuel saving effect of the 12 V/70 Ah HSC. Furthermore, the average starting fuel consumption of the 12 V/50 Ah HSC and 12 V/70 Ah LFP battery module was between 2.9 mL and 3 mL. In addition, its fuel saving effect was between 12 V/70 Ah HSC and 12 V/70 Ah VRLA battery module. The 12 V/70 Ah VRLA battery module had an eighth start fuel consumption of 3.25 mL or more possibly due to slow VRLA battery module voltage recovery. As a result, exceedingly low voltage and a small current were produced, thus increasing the startup time.

Table 8 Comparison and analysis of four energy storage systems in multiple starts modes.

Data	12 V/70 Ah HSCs	12 V/50 Ah HSCs	12 V/70 Ah LFP batteries	12 V/70 Ah VRLA batteries
Mean startup time (s)	1.567	1.658	1.669	1.926
Average startup fuel consumption (mL)	2.864	2.912	2.958	3.107

Idle fuel consumption flow rate (mL/min)	72	72	72	72

As demonstrated in Table 8, the average starting time and average starting fuel consumption of the four energy storage systems are different to a certain extent. As compared to the 7.82% fuel saving of the VRLA battery module, the 12 V/70 Ah HSC had the most obvious fuel-saving effect. As compared with LFP battery module, the fuel saving effect was reduced by 3.18%. In comparison with the 12 V/50 Ah HSC, the fuel saving effect was weak (1.65%).

3.4. Startup exhaust analysis

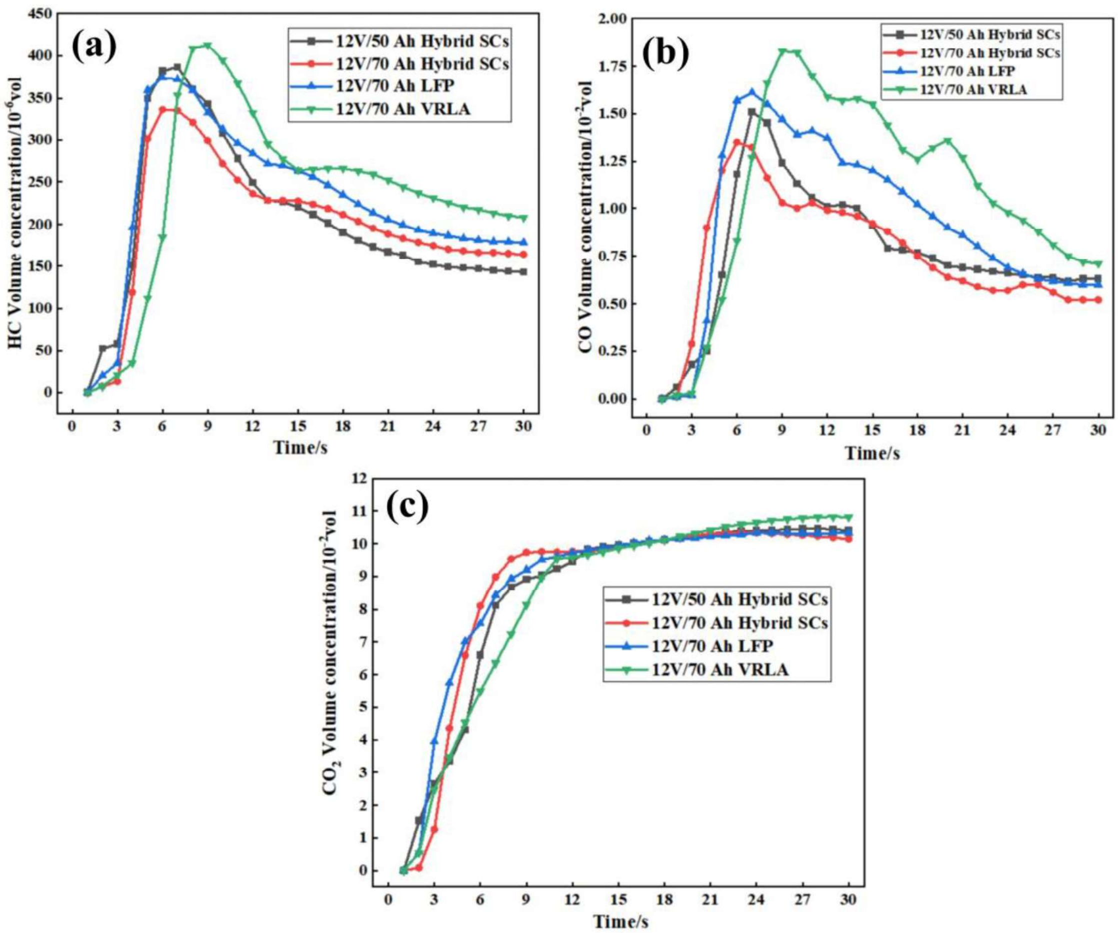

Fig. 10. The tail gas curves of four energy storage systems in multiple startup: (a) HC volume concentration; (b) CO volume concentration, and (c) CO_2 volume concentration.

The tail gas of the four energy storage systems in multiple startup experiments were analyzed (Fig. 10a). The volume concentration of HC was the lowest in the starting process of 12 V/70 Ah HSC. The volume concentration of HC in the starting process of 12 V/50 Ah HSC was close but slightly higher to that of the 12 V/70 Ah LFP battery module. In addition, the maximum HC volume concentration of the 12 V/70 Ah VRLA battery module reached 420×10^{-6} vol during startup. However, the HC volume concentration first rose sharply and then exhibited a slow decline due to engine starting. As such, the burning temperature was lower and the residual gas in cylinder quantity was large, thereby creating a relatively rich mixture and causing insufficient combustion and larger HC emission concentration. At a stable operation, flow mixing in the cylinder was disturbed, such that increased eddy diffusion promoted burning and reduced the HC emission concentration. The low volume concentration of HC when the 12 V/70 Ah HSC started was due to the larger instantaneous power, shorter startup time, and faster starting. This allowed faster starting to reach a stable speed to promote combustion and lower the volume concentration of HC.

Fig. 10b presents the starting process, where the volume concentration of CO rose sharply at first, decreased slowly, and gradually stabilized. The start engine speed was lower, the volume was limited, thereby creating a rich mixture that affected the concentration of CO generated by the mixture concentration. However, not enough oxygen was allowed for the fuel carbon combustion into CO_2, thus generating a large amount of CO. Afterwards, the engine speed increased to a stable operation, thereby increasing the volume and expanding the oxygen content to promote carbon transformation into CO_2. This ultimately resulted in a decrease in the CO content. The CO volume concentration was the lowest when the 12 V/70 Ah HSC first started, and the CO volume concentration was higher when the 12 V/50 Ah HSC and the 12 V/70 Ah LFP battery module started. However, the volume concentration of HC was the highest when 70 Ah VRLA battery module started. In addition, the time to reach the maximum value had a certain delay. The 12 V/70 Ah HSC released a larger current and smaller voltage drop when starting, which resulted in a larger instantaneous starting power and a rapid increase in the starting speed. As a result, the air intake and the content of oxygen increased, thereby producing fuller carbon combustion and enhanced conversion into CO_2. These resulted in a lower CO and better emission reduction effects during the startup process.

According to Fig. 10c, on the whole, the volume concentration of CO_2 rose sharply at first and then slowly increased. The volume concentration of CO_2 continuously increase with the rapid increase of engine speed at the beginning of startup. As the engine gradually stabilized, the volume concentration of CO_2 rose slowly and stabilized at a certain value. The CO_2 volume concentration was significantly higher when the 12 V/70 Ah HSC was started. In addition, the CO_2 volume concentration was lower when 12 V/50 Ah HSC and 12 V/70 Ah LFP battery module were started. In comparison, the CO_2 volume concentration was the lowest when 12 V/70 Ah VRLA battery module was started. This was mostly predominant when the 12 V/70 Ah HSCs were started, which resulted in a fuller HC combustion, higher carbon combustion, and more CO_2, ultimately increasing the volumetric concentration of CO_2.

4. Conclusions and future recommendations

4.1. Conclusions

Based on the HSC, a set of 12 V / 50 Ah and 12 V/70 Ah energy storage systems were designed in this paper, which were assembled and tested. Through the starting performance, energy-saving and emission-reduction experiments, the 12 V/70 Ah VRLA battery module and 12 V/70 Ah LFP battery module were compared, from which the following conclusions were drawn:

(1) An electrochemical performance test was performed on the self-designed HSC energy storage system. The results indicated that the charging/discharging characteristics of 12 V/50 Ah and 12 V/70 Ah HSC were consistent. The charging/discharging voltage first jumped up or down and then slowly changed to the cut-off voltage, which reflects the high

energy characteristics of the combination of the SC and battery. In addition, the actual capacity of the energy storage system met the design requirements.

(2) As compared to the starting of 12 V/70 Ah VRLA battery module and 12 V/70 Ah LFP battery module, the starting instant release current of the 12 V/70 Ah HSC was larger, the voltage drop was smaller, and the starting instantaneous power was larger. These were beneficial for rapid starting and reducing the sense of frustration. However, as the starting torque increased, the resulting starting noise also increased. In addition, the 12 V/50 Ah and 12 V/70 Ah HSCs started to release currents at a similar speed. The voltage rose significantly and the current consistently changed during the charging phase, which was conducive to absorbing current.

(3) From the fuel consumption experimental data, the starting time of the 12 V/70 Ah HSC was short, and the fuel consumption during stable operation was 72 mL/min. As compared to the 12 V/70 Ah VRLA battery module, the fuel-saving effect was the most obvious. As compared to the 12 V/70 Ah LFP battery module, the fuel-saving effect decreased by 3.18%. Compared with the 12 V/50 Ah HSC, the fuel-saving effect was not obvious. On the whole, it showed good fuel economy.

(4) Hence, through the analysis of experimental data, it can be concluded that the volume concentration of HC and CO in the tail gas was low and the concentration of CO_2 was high when the 12 V/70 Ah hybrid HSC started, indicating that the fuel combustion was more sufficient during startup and had obvious emission-reduction effects

4.2. Future recommendations

Based on the above review and analysis, the following future development opportunities and challenges of HSC energy storage system are suggested:

(1) Considering the needs of high starting power and long-term continuous power, HSC combine the advantages of high-power density and high-energy

density. In addition, they have superior starting performance as an automotive energy storage system. It is worth noting that improving the energy density while keeping the power density as high as possible will be one of the hot spots in future research.

(2) As a kind of vehicle startup energy storage system, the problems of startup time, startup frustration, and energy decay during frequent startup will directly affect the user's experience. Therefore, during the startup process, future research should focus on the aging of energy storage systems and performance degradation. Considering the actual operating conditions of the vehicle (climbing, acceleration, starting, collision, low temperature), the starting performance of the complex environment is worth further exploration.

(3) When a car starts to stumble, it will consume more fuel, and the main reason for the slump is the lack of power supply from the energy storage system. Therefore, a HSC energy storage system with high energy density and low self-discharge rate needed to reduce fuel consumption. In addition, HSC will be the most promising future energy storage system application solution in automotive energy recovery systems.

(4) Reducing exhaust emissions is also a key factor to measure the starting performance of vehicles. The superior emission reduction performance of HSCs is more conducive to green environmental protection, but other components of exhaust also need to be further studied. In addition, the development of a high-performance, high-security, low-cost, and maintenance-free energy storage system is of urgent need.

Acknowledgements

This research was financially supported by the National Natural Science Foundation of China (Grant No. 51906047), Guangdong Basic and Applied Basic Research Foundation (Grant No.2021B1515130008), Zhuhai Science and Technology

Project (Grant No.2H2203620121015PWC), Zhuhai Science and Technology Planning Project in the Field of Social Development (Grant No.2220004000343).

References

[1] Ravindranath TY, RamaKoteswara RA, Rajani K, et al. Super capacitors for energy storage: Progress, applications and challenges. J Energy Storage 2022;49:104194.

[2] Ahmed A, Sheikh MHR, Atia TA, et al.Advanced materials and technologies for hybrid supercapacitors for energy storage - A review. J Energy Storage 2019;25:100852.

[3] Li Q, Su B, Pu Y, et al. A state machine control based on equivalent consumption minimization for fuel cell/supercapacitor hybrid tramway. IEEE Trans Transp Electrif 2019;5:552-64.

[4] Chen XL,Paul R,Dai LM. Carbon-based supercapacitors for efficient energy storage. Natl Sci Rev 2017;403:453-89.

[5] Shao YL, El-Kady MF, Sun JY, et al. Design and Mechanisms of Asymmetric supercapacitors. Chem Rev 2018;118(18):9233-80.

[6] Wang Y, Sun Z, Chen Z, et al. Energy management strategy for battery/supercapacitor/fuel cell hybrid source vehicles based on finite state machine. Appl Energ 2019;254:113707.

[7] Li Q, Yang H, Han Y, et al. A state machine strategy based on droop control for an energy management system of PEMFC-battery-supercapacitor hybrid tramway. Int J Hydrogen Energy 2016;41:16148-59.

[8] Qian X, Stefan L, Liu YJ. Design and experimental verification of a fuel cell/supercapacitor passive configuration for a light vehicle. J Energy Storage 2021;33:102110.

[9] Liu H, Wei L, Wang H. Review on reliability of supercapacitors in energy storage applications. Appl Energ 2020;278:115436.

[10] Devi N, Ray SS. Performance of bismuth-based materials for supercapacitor applications: A review. Mater Today Commun 2020;25:101691.

[11] Beywardnan DBW, Hredzak B, Agelidis VG. Supercapacitor sizing method for energy-controlled filter-based hybrid energy storage systems. IEEE T Power Electr 2017;322:1626-37.

[12] Dubal DP, Ayyad O, Ruiz V, et al. Hybrid energy storage: the merging of battery and supercapacitor chemistries. Chem Soc Rev 2015;44: 24965731.

[13] Noori AE, Kady MF, Rahmanifar MS, et al. Towards establishing standard performance metrics for batteries, supercapacitors and beyond. Chem Soc Rev 2019;48:1272-1341.

[14] Wang J, Li Q, Peng C, et al. To increase electrochemical performance of electrode material by attaching activated carbon particles on reduced graphene oxide sheets for supercapacitor. J Power Sources 2020;450:227611.

[15] Jing W, Lai CH, Wong WSH, et al. A comprehensive study of battery-supercapacitor hybrid energy storage system for standalone PV power system in rural electrification. Appl Energ 2018;224:340-56.

[16] Wang YG, Song YF, Xia YY. Electrochemical capacitors: mechanism, materials, systems, characterization and applications. Chem Soc Rev 2016;45 (21):5925-50.

[17] Minho KIM, Fan XU, Le JH, et al. A fast and efficient pre-doping approach to high energy density lithium-ion hybrid capacitors. J Mater Chem A 2014;226:10029-33.

[18] Annadanesh S, Daniel A, et al. Investigation of pre-lithiation in graphite and hard-carbon anodes using different lithium source structures. J Electrochem Soc 2017;164:3914-24.

[19] Zheng JS, Zhang L, Annadanesh S, et al. A hybrid electrochemical device based on a synergetic inner combination of Li ion battery and Li ion capacitor for energy storage. Sci Rep-UK 2017;7:419101-8.

[20] Zhang S, Xiong R, Sun F, et al. Model predictive control for power management in a plug-in hybrid electric vehicle with a hybrid energy storage system. Appl Energ 2017:1654-62.

[21] Both J. The modern era of aluminum electrolytic capacitors. IEEE Electr Insul M 2018;314:24-34.

[22] Krishnamoorthy K, Pazhamalai P, Mariappan V, et al. Probing the energy conversion process in piezoelectric-driven electrochemical self-charging supercapacitor power cell using piezoelectrochemical spectroscopy. Nat Commun 2020;11:2351.

[23] Qin H, Liu P, Chen C, et al. A multi-responsive healable supercapacitor. Nat Commun 2021;12:4297.

[24] Wei Z, Liu T, Zhang L, et al. Sulfide-Based Nickel-Plated Fabrics for Foldable Quasi-Solid-State Supercapacitors. Energy Environ Mater 2022;5:883-891.

[25] Lia K, Wahiba Y, Evgueniy E. Hybrid battery/supercapacitor energy storage system for the electric vehicles. J Power Sources 2018;374:237-48.

[26] Ali N, Liu ZZ, Armghan H, et al. Double integral sliding mode controller for wirelessly charging of fuel cell-battery-super capacitor based hybrid electric vehicle. J Energy Storage 2022;51:104288.

[27] Yuan J, Yang L, Chen Q, et al. Intelligent energy management strategy based on hierarchical approximate global optimization for plug-in fuel cell hybrid electric vehicles. Int J Hydrogen Energy 2018;43:8063-78.

[28] Tribioli L, Cozzolino R, Chiappini D, et al. Energy management of a plug-in fuel cell/battery hybrid vehicle with on-board fuel processing. Appl Energ 2016:140-54.

[29] Dubal DP, Ayyad O, Ruiz V, et al. Hybrid energy storage: The merging of battery and supercapacitor chemistries. Chem Soc Rev 2015;447:1777-90.

[30] Yan Y, Li Q, Chen W, et al. Optimal energy management and control in multimode equivalent energy consumption of fuel cell/supercapacitor of hybrid electric tram. IEEE T Ind Electron 2019;66:6065-76.

[31] Yang J, Hu C, Wang H. Review on the research of failure modes and mechanism for lead-acid batteries. Int J Energ Res 2017;413:336-52.

[32] Li B, Dai F, Xiao QF, et al. Nitrogen-dopedactivated carbon for a high energy hybrid supercapacitor. Energ Environ Sci 2016;91:102-6.

[33] Cao WJ, Zheng JS, Adams D, et al. Comparative study of the power and cycling performance for advanced lithiumion capacitors with various carbon anodes. J Electrochem Soc 2014;161:2087-92.

[34] Geng B, Mills JK, Sun D, et al. Combined power management/design optimization for a fuel cell/battery plug-in hybrid electric vehicle using multi-objective particle swarm optimization. Int J Auto Tech-Kor 2014;15(4):645-54.

[35] Ettihir K, Boulon L, Agbossou K, et al. Optimization-based energy management strategy for a fuel cell/battery hybrid power system. Appl Energ 2016:142-53.

[36] Sun J, Xu C, Chen H. A review on the synthesis of $CuCo_2O_4$-based electrode materials and their applications in supercapacitors. J Materiomics 2021;7:98-126.

[37] Liu D, Liu Y, Liu X, et al. Growth of uniform $CuCo_2O_4$ porous nanosheets and nanowires for high-performance hybrid supercapacitors. J Energy Storage 2022;52:105048.

[38] Sun J, Du X, Wu R, et al. Bundlelike $CuCo_2O_4$ Microstructures Assembled with Ultrathin Nanosheets As Battery-Type Electrode Materials for High-Performance Hybrid Supercapacitors. ACS Appl Energ Mater 2020;3:8026-8037.

[39] Jing W, Hung C, Wong WSH, et al. Dynamic power allocation of battery-supercapacitor hybrid energy storage for standalone PV microgrid applications. Sustainable Energy Technol Assess 2017;22:55-64.

[40] Sinha S, Bajpai P. Power management of hybrid energy storage system in a standalone DC microgrid. J Energy Storage 2020;30:101523.

[41] Wang HY, Li XL, Jiang DQ, et al. Organohydrogel electrolyte-based flexible zinc-ion hybrid supercapacitors with dendrite-free anode, broad temperature adaptability and ultralong cycling life. J Power Sources 2022;528:231210.

[42] Liu YC, Miao XF, Zhang XX, et al. High performance flexible quasi-solid-state zinc-ion hybrid supercapacitors enable by electrode potential adjustment, J Power Sources 2021;495:229789.

[43] Lee G, Jang J. High-performance hybrid supercapacitors based on novel $Co_3O_4/Co(OH)_2$ hybrids synthesized with various-sized metal-organic framework templates. J Power Sources 2019;423:115-24.

[44] Chen H, Du X, Liu X, et al. Facile growth of nickel foam-supported $MnCo_2O_{4.5}$ porous nanowires as binder-free electrodes for high-performance hybrid supercapacitors. J Energy Storage 2022;50:104297.

[45] Liu Y, Du X, Li Yi, et al. Nanosheet-assembled porous $MnCo_2O_{4.5}$ microflowers as electrode material for hybrid supercapacitors and lithium-ion batteries. J Colloid Interf Sci 2022;627:815-826.

[46] Wu R, Sun J, Xu C, et al. $MgCo_2O_4$-based electrode materials for electrochemical energy storage and conversion: a comprehensive review. Sustain Energ Fuels 2021;5:4807-4829.

[47] Yin X, Han L, Fu Y et al. $(Ni,Co)Se_2$ nanoparticles on vertical graphene nanosheets@carbon microtubes for high-performance solid-state asymmetric supercapacitors. J Energy Storage 2022;53:105205.

[48] Zou Y, Liu T, Liu D, et al. Reinforcement learning-based real-time energy management for a hybrid tracked vehicle. Appl Energ 2016:372-82.

[49] Li H, Ravey A, Diaye AN, et al. A novel equivalent consumption minimization strategy for hybrid electric vehicle powered by fuel cell, battery and supercapacitor, J Power Sources 2018;395:262-70.

[50] Liu T, Zou Y, Liu D, et al. Reinforcement learning of adaptive energy management with transition probability for a hybrid electric tracked vehicle. IEEE T Ind Electron 2015;62:7837-46.

[51] Mandal D, Jeong JY, Singu BS, et al. Flexible all solid-state niobium nitride//activated carbon lithium-ion hybrid capacitor with high volumetric power and energy densities. J Energy Storage 2022;48:104031.
[52] Guentri H, Allaoui T, Mekki M, et al. Power management and control of a photovoltaic system with hybrid battery-supercapacitor energy storage based on heuristics methods. J Energy Storage 2021;39:102578.
[53] Pedro J, Corral V, Luis M, et al. Hybrid powertrain, energy management system and techno-economic assessment of rubber tyre gantry crane powered by diesel-electric generator and supercapacitor energy storage system. J Power Sources 2019;412:311-20.
[54] Shao Y, El-Kady MF, Sun J, et al. Design and mechanisms of asymmetric supercapacitors. Chem Rev 2018;118:9233-80.
[55] Ren G, Wang H, Chen C, et al. An energy conservation and environmental improvement solution-ultra-capacitor/battery hybrid power source for vehicular applications. Sustain Energy Techn 2021;44:100998.
[56] Burke A, Miller M. The power capability of ultracapacitors and lithium batteries for electric and hybrid vehicle application. J Power Sources 2011;196:514-22.
[57] Kouchachvili L, Yaïci W, Entchev E. Hybrid battery/supercapacitor energy storage system for the electric vehicles. J Power Sources 2018;374:237-48.
[58] Cheng C, Wei C, He Y, et al. Etching strategy synthesis of hierarchical ni-mn hydroxide hollow spheres for supercapacitors. J Energy Storage 2021;33:102105.
[59] Satpathy S, Das S, Bhattacharyya BK. How and where to use super-capacitors effectively, an integration of review of past and new characterization works on super-capacitors. J Energy Storage 2020;27:101044.
[60] Fletcher TP, Thring RH, Watkinson M, et al. An energy management strategy to concurrently optimise fuel consumption & PEM fuel cell lifetime in a hybrid vehicle. Int J Hydrogen Energ 2016;41:21503-15.

[61] Bizon Nicu. Real-time optimization strategies of Fuel Cell Hybrid Power Systems based on Load-following control: a new strategy, and a comparative study of topologies and fuel economy obtained. Appl Energ 2019;241:444-60.

[62] Mwambeleko JJ, Kulworawanichpong T. Battery electric multiple units to replace diesel commuter trains serving short and idle routes. J Energy Storage 2017;11:7-15.

[63] Sengupta AS, Satpathy S, Mohanty SP, et al. Supercapacitors outperform conventional batteries. IEEE Consum Electron Mag 2018;7:50-3.

[64] Raghavendra KVG, Vinoth R, Zeb K, et al. An intuitive review of supercapacitors with recent progress and novel device applications. J Energy Storage 2020;31:1-34.

[65] Sharma K, Arora A, Tripathi SK. Review of supercapacitors: materials and devices. Cureus J Med Science 2019;21:801-5.

[66] Ouyang M, Zhang W, Wang E, et al. Performance analysis of a novel coaxial power-split hybrid powertrain using a CNG engine and supercapacitors. Appl Energ 2015;157:595-606.

[67] Zhang S, Xiong R. Adaptive energy management of a plug-in hybrid electric vehicle based on driving pattern recognition and dynamic programming. Appl Energ 2015:68-78.

[68] Peng H, Wang J, Shen W, et al. Controllable regenerative braking process for hybrid battery/ultracapacitor electric drive systems. IET Power Electron 2018;11:2507-14.

[69] Khademi B, Nateghi MR, Shayesteh MR, et al. High voltage binder free hybrid supercapacitor based on reduced graphene oxide/graphene oxide electrodes and “water in salt” electrolyte. J Energy Storage 2021;43:103164.

[70] Li Q, Wang T, Dai C, et al. Power management strategy based on adaptive droop control for a fuel cell-battery-supercapacitor hybrid tramway. IEEE Trans Veh Technol 2018;67:5658-70.

[71] Benoy SM, Pandey M, et al. Recent trends in supercapacitor-battery hybrid energy storage devices based on carbon materials. J Energy Storage 2022;52:104938.

[72] Wang Y, Yang Z, Li F. Optimization of energy management strategy and sizing in hybrid storage system for tram. Energies 2018;11:741-52.

[73] Joachim J, MwambelekoTK. Supercapacitor and accelerating contact lines hybrid tram system. J Energy Storage 2021;44:103277.

[74] Zhang Q, Wang L, Li G, et al. A real-time energy management control strategy for battery and supercapacitor hybrid energy storage systems of pure electric vehicles. Cureus J Med Science 2020;31:101721.

[75] Shayeghi H, Monfaredi F, Dejamkhooy A, et al. Assessing hybrid supercapacitor-battery energy storage for active power management in a wind-diesel system. Int J Elec Power 2021;125:106391.

[76] Li X, Wang Y, Yang D, et al. Adaptive energy management strategy for fuel cell/battery hybrid vehicles using Pontryagin's Minimal Principle. J Power Sources 2019;440:227105.

[77] Wieczorek M, Lewandowski M. A mathematical representation of an energy management strategy for hybrid energy storage system in electric vehicle and real time optimization using a genetic algorithm. Appl Energ 2017;192:222-33.

[78] Golchoubian P, Azad NL. Real-time nonlinear model predictive control of a battery-supercapacitor hybrid energy storage system in electric vehicles. IEEE T Veh Technol 2017;66(11):9678-88.

[79] Zhang Q, Deng W, Li G. Stochastic control of predictive power management for battery/supercapacitor hybrid energy storage systems of electric vehicles. IEEE T Ind Inform 2017;14:3023-30.

[80] Dubal DP, Ayyad O, Ruiz V, Gomez-Romero P. Hybrid energy storage: the merging of battery and supercapacitor chemistries. Chem Soc Rev 2015;44:1777-90.

[81] Chen GZ. Supercapacitor and supercapattery as emerging electrochemical energy stores. Int Mater Rev 2017;62:173-202.

[82] Shao Y, El-Kady MF, Sun J, et al. Design and mechanisms of asymmetric supercapacitors. Chem Rev 2018;118:9233-80.

[83] Liu Q, Zhu H, Ma Q, et al. Ultrathin MoS_2 nanosheets hybridizing with reduced graphene oxide for high-performance pseudocapacitors. FlatChem 2020;26:100212.

[84] Sun ZD, Wang YJ, Chen ZH, et al. Min-max game based energy management strategy for fuel cell/supercapacitor hybrid electric vehicles. Appl Energ 2020;267:115086.

[85] Li Q, Yang H, Han Y, et al. A state machine strategy based on droop control for anenergy management system of PEMFC-battery-supercapacitor hybrid tramway. Int J Hydrogen Energ 2016;41:16148-59.

[86] Zhu T, Richard GA, Roberto L, et al. Adaptive energy management of a battery-supercapacitor energy storage system for electric vehicles based on flexible perception and neural network fitting. Appl Energ 2021;292:116932.

[87] Ostadi A, Kazerani M. A comparative analysis of optimal sizing of battery-only, ultracapacitor-only, and battery-ultracapacitor hybrid energy storage systems for a city bus. IEEE T Veh Technol 2015;64:4449-60.

[88] Song ZY, Hofmann H, Li J, et al. Energy management strategies comparison for electric vehicles with hybrid energy storage system. Appl Energ 2014;134:321-31.

[89] Raza W, Ali F, Raza N, et al. Recent advancements in supercapacitor technology. Nano Energy 2018;52:441-73.

[90] Xiao J, Li Q, Bi Y, et al. Understanding and applying coulombic efficiency in lithium metal batteries. Nat Energy 2020;5:561-568.

[91] Bi T, Chen H, Li J, et al. A novel hierarchical porous carbon-supported MnO_2 nanofibers composite with three-dimensional interpenetrating network structure as a high-performance supercapacitor. Electrochim Acta 2022;433:141266.